Water Supersaturation for Early Mars

A. Delavois, F. Forget, M. Turbet, E. Millour, R. Vandemeulebrouck, L. Lange, A. Bierjon

JGR Planets

RESEARCH ARTICLE
10.1029/2022JE007424

Water Supersaturation for Early Mars

A. Delavois[1], F. Forget[1], M. Turbet[1], E. Millour[1], R. Vandemeulebrouck[1], L. Lange[1], and A. Bierjon[1]

[1]Laboratoire de Météorologie Dynamique/IPSL, Sorbonne Université, ENS, PSL Research University, Ecole Polytechnique, CNRS, Paris, France

Key Points:

- We simulated water supersaturation in an early Mars climate considering an abundant source of water on the surface and an arid scenario
- Supersaturation can warm early Mars only with unrealistic supersaturation ratios
- Supersaturation is only efficient when it occurs in the lower layers of the atmosphere in our simulations

Correspondence to:

A. Delavois,
antony.delavois@lmd.ipsl.fr

Citation:

Delavois, A., Forget, F., Turbet, M., Millour, E., Vandemeulebrouck, R., Lange, L., & Bierjon, A. (2023). Water supersaturation for early Mars. *Journal of Geophysical Research: Planets*, *128*, e2022JE007424. https://doi.org/10.1029/2022JE007424

Received 7 JUN 2022
Accepted 2 JUN 2023

Abstract Evidence of past liquid water flowing on the surface of Mars has been identified since the first orbital mission to the planet. However, reconstructing the climate that would allow liquid water at the surface is still an intense area of research. Previous studies showed that an atmosphere composed only of CO_2 and H_2O could not sustain surface temperatures above the freezing point of water. Different solutions have been studied, ranging from events like impacts on different atmospheric compositions, or even radiative feedback of water clouds that would create a dramatic greenhouse effect. In this context, we propose to study whether the supersaturation of water could warm the planet. Strong supersaturation is observed in the present-day Martian atmosphere. On early Mars, supersaturation could enhance the greenhouse effect through strong absorption of the IR flux by water vapor or by modifying water clouds. While 1D modeling suggests a significant impact, our 3D model shows that warming the climate of early Mars requires a high supersaturation ratio, especially in the lower layers of the atmosphere. This configuration seems highly unrealistic since the level of supersaturation is higher than what would be expected in a dense atmosphere.

Plain Language Summary Mars around 4 billion years ago is thought to have had a more Earth-like climate with liquid water on its surface. Today's observations show evidence for past valleys, riverbeds, and lakes, suggesting that past conditions would have been potentially habitable on the Red Planet. This tremendous scene is, however, not well understood, since a dramatic greenhouse effect would have been needed. Previous studies were not convincing enough to predict a warm and wet climate during the Noachian/Hesperian period on Mars. Water supersaturation means that there was more water vapor in the air than could usually be held by the atmosphere, causing an eventual stronger greenhouse effect. Also, a potential modification to water clouds could have an additional warming effect. Using state-of-the-art climate models, we investigate the potential role of water supersaturation on the climate of early Mars, without tackling the question of its origin. Our results show that unrealistic supersaturation conditions would be needed to reach an atmosphere with a global temperature that could host liquid water. Considering that the lower layers of the atmosphere could not host such an amount of water vapor, we conclude that the supersaturation of the atmosphere is unlikely to be the solution to the early Mars enigma.

1. Introduction

Rovers and orbiters sent to Mars have provided us with compelling evidence for abundant liquid water flowing on the surface in the early days of the planet, during the Noachian and Hesperian eras. One of the biggest challenges in planetary science is to reconcile these geological and mineralogical features with a corresponding warm climate despite a fainter Sun irradiating Mars with less than a third of today's Earth-received energy (Gough, 1981; Sagan & Mullen, 1972). Some recent studies found that the greenhouse effect of a reduced thick atmosphere, mainly composed of CO_2, H_2O, and H_2, could sustain a warm climate for periods long enough to explain the presence of valley networks (Kamada et al., 2021; Ramirez, 2017; Ramirez et al., 2014; Turbet & Forget, 2022; Wordsworth, 2016). However, explaining the entire Noachian/Hesperian era only with this scenario is unlikely since dramatic climate changes must have occurred during this 1-Gy long period. For instance, it is difficult to reconcile the presence of Mn-rich rocks, which could only be created within a wet and oxidized environment, with a significant amount of H_2 in the atmosphere (Lanza et al., 2016). This is one reason to keep searching for new processes or events that can be responsible for a substantial greenhouse effect.

A recent study suggests that H_2O_2 could have provided a sufficient greenhouse effect, assuming that H_2O_2 supersaturation occurs in the upper layers of the atmosphere (Ito et al., 2020). Given that water can be much more abundant and can absorb in the same window as H_2O_2, what about water supersaturation?

Moreover, supersaturation could have an effect on clouds by raising the hygropause. It would create higher and cooler clouds with a subsequently stronger greenhouse effect, leading to a potential warming of the surface. The cirrus cloud greenhouse warming hypothesis has been previously studied, first in the context of a post-impact climate (Segura et al., 2002, 2008, 2012) showing promising results for maintaining a warm climate over a relatively long period, although this was shown to be overestimated by Turbet et al. (2017) because of convection and condensation processes. Other studies suggest that clouds could provide warming but only under very specific assumptions on microphysics or ice location (Kite et al., 2021; Ramirez & Kasting, 2017; Urata & Toon, 2013).

On current-day Mars, water exceeding saturation levels has been observed in the atmosphere (Fedorova et al., 2018, 2020; Maltagliati et al., 2011), and is sometimes associated with the formation of water clouds. Supersaturation ratios are able to reach as much as 10 around 30–40 km (Maltagliati et al., 2011) and even up to 300 in the upper atmosphere of Mars, around 80 km (Fedorova et al., 2020). It has been observed that supersaturation in the top part of cirrus clouds is enhanced during the dusty season and, in particular, during Global Dust Storms, reaching a ratio of 5 at approximately 60–70 km (Poncin et al., 2022).

This phenomenon is also observed in the upper troposphere of the Earth, and is mostly associated with the formation of cirrus clouds (Heymsfield et al., 2017; Krämer et al., 2020). It has also been observed near the surface on the icy desert of Antarctica (Genthon et al., 2017). Supersaturation ratios in cirrus clouds are limited by the formation of ice particles from either homogeneous or heterogeneous nucleation (Baumgartner et al., 2022; Vali et al., 2015). Relative humidity in these conditions does not exceed 200% (Krämer et al., 2009; Lamquin et al., 2012), which is also the order of magnitude observed in Antarctica (Genthon et al., 2017). Some water ice particles are sometimes found in the summertime high-latitude mesosphere, creating supersaturation ratios exceeding 10^5, giving birth to noctilucent clouds (Murray & Jensen, 2010). This ratio is constrained by homogeneous nucleation from the vapor phase and thus can be considered as an extreme upper limit for our study. However, reaching these levels of saturation in the lower atmosphere seems unrealistic.

In this paper, using 1D and 3D climate models, we try to establish the potential of water supersaturation to warm the surface of early Mars. We do not consider any a priori assumption concerning supersaturation limitation or origin, except that the source of water is located at the surface of the planet for the 3D simulations. We tested two sets of simulations in order to explore the sensitivity to available water, with a relatively arid simulation and an idealistic, extremely wet simulation.

2. Methods

2.1. General Description

For this study, we used the Generic Planetary Climate Model (Generic PCM, previously LMD Generic Global Climate Model) both in its 1D and 3D versions, adapted to typical Noachian conditions. Early Mars climates have already been studied with this model, including full CO_2 and water cycles (Forget et al., 2013; Turbet & Forget, 2019, 2022; Turbet et al., 2017; Wordsworth et al., 2013), and a full description of the model can be found in Forget et al. (2013) and Wordsworth et al. (2013). We assume a mean surface pressure of 2 bar because it is the optimum pressure for warming an atmosphere mainly composed of CO_2 (Forget et al., 2013, Figure 1). The solar flux is set to 75% of today's Mars received flux, giving a mean solar flux on Mars of 111 W/m^2.

This paper first presents global averaged 1D simulations vertically divided into 34 layers (up to ~1 Pa or 100 km). Water is considered only as a radiatively active gas in the atmospheric composition. We do not consider a full water cycle, since evaporation, condensation and rain are neglected in the 1D simulations. The effects of water clouds are not included in the 1D simulations for the sake of simplicity in the interpretation of results since we do not consider a full water cycle. We further explore the role of water clouds by implementing a full water cycle in the 3D simulations. However, CO_2 clouds are taken into account and CO_2 microphysics are performed with a cloud condensation nuclei number density of 1,000 particles per kilogram of Martian atmosphere. We tuned this parameter in order to model a global greenhouse effect analogous to the one obtained in 3D by Wordsworth et al. (2013).

Three-dimensional simulations were performed with a horizontal resolution of 11.25° (32 × 32 in longitude × latitude). The vertical dimension is split into 15 layers with the top layer at ~1,000 Pa. Vertical layers are described using hybrid coordinates.

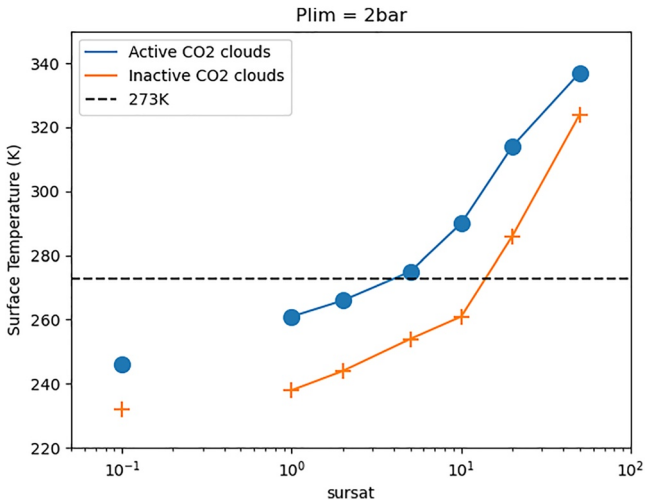

Figure 1. Surface temperature as a function of supersaturation ratio for 1D simulation. Supersaturation is allowed down to the surface (*plim* = p_s). Surface pressure is 2 bar. Note that the 10^{-1} points represent dry simulations and are given for reference.

We used the pre-true polar wander (pre-TPW) topography from Bouley et al. (2016) that demonstrated that the formation of late Noachian valley networks is likely to have predated the formation of most of the Tharsis volcanic bulge. The pre-TPW topography is based on present-day MOLA topography but without Tharsis and all the younger volcanic features. It also takes into account that a TPW event of 20°–25° occurred during the rise of Tharsis. A topography without Tharsis could potentially have an effect on the climate since the high-altitude bulge acts like a cold-trap and then modify the climate with the ice-albedo feedback. Moreover, topography can drive the precipitation patterns, as demonstrated in Turbet and Forget (2022).

Because the water content during the Noachian era was poorly constrained, we explored two different scenarios for available water in the climate system. First, we use a relatively dry initial state where ice is mainly located in cold traps, that is, high altitude areas and poles. This initial state comes from the simulation presented in Bouley et al. (2016, Figure 2b) and is therefore considered to be realistic, although it was done for a mean surface pressure of 0.2 bar. The global equivalent layer (GEL) of ice is approximately 37 mm thick.

The other set of 3D simulations is performed with an idealized wet set-up designed to overestimate the amount of water vapor in the atmosphere and thus the greenhouse effect. We initialize simulations with a global ice sheet of 10 m covering the entire planet. In order to maximize water in the atmosphere, we set the albedo of the ice to 0.2, which is usually the albedo of bare ground. Combined with an obliquity of 40°, favoring water transport, these simulations are designed to explore the supersaturation scenario for an idealized, extremely wet case.

2.2. Modeling Supersaturation

2.2.1. Supersaturation in the 1D Model

Supersaturation is implemented in a simple way for 1D simulations. At the end of each time step, we calculate the water mass mixing ratio at saturation in each layer using the Clausius-Clapeyron equation. Then, this mass mixing ratio of water is multiplied by the prescribed supersaturation ratio (*sursat* parameter). A pressure limit of supersaturation (*plim*) is added to the model in order to allow supersaturation only above a certain level, since

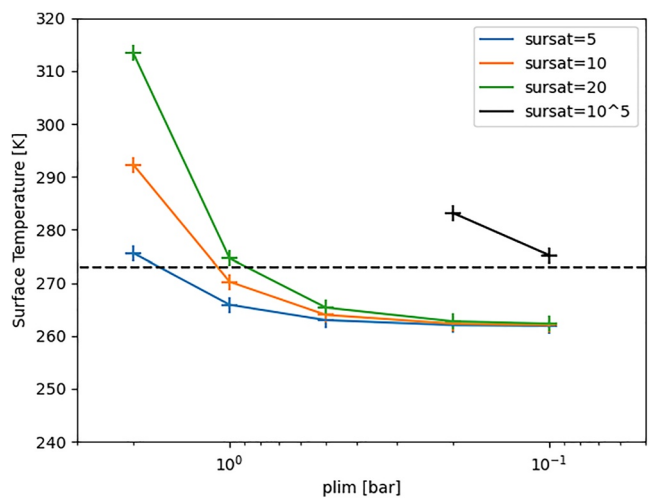

Figure 2. Surface temperature as a function of the pressure limit of supersaturation (*plim*) for 1D simulation and for different supersaturation ratios(*sursat*). Surface pressure is 2 bar.

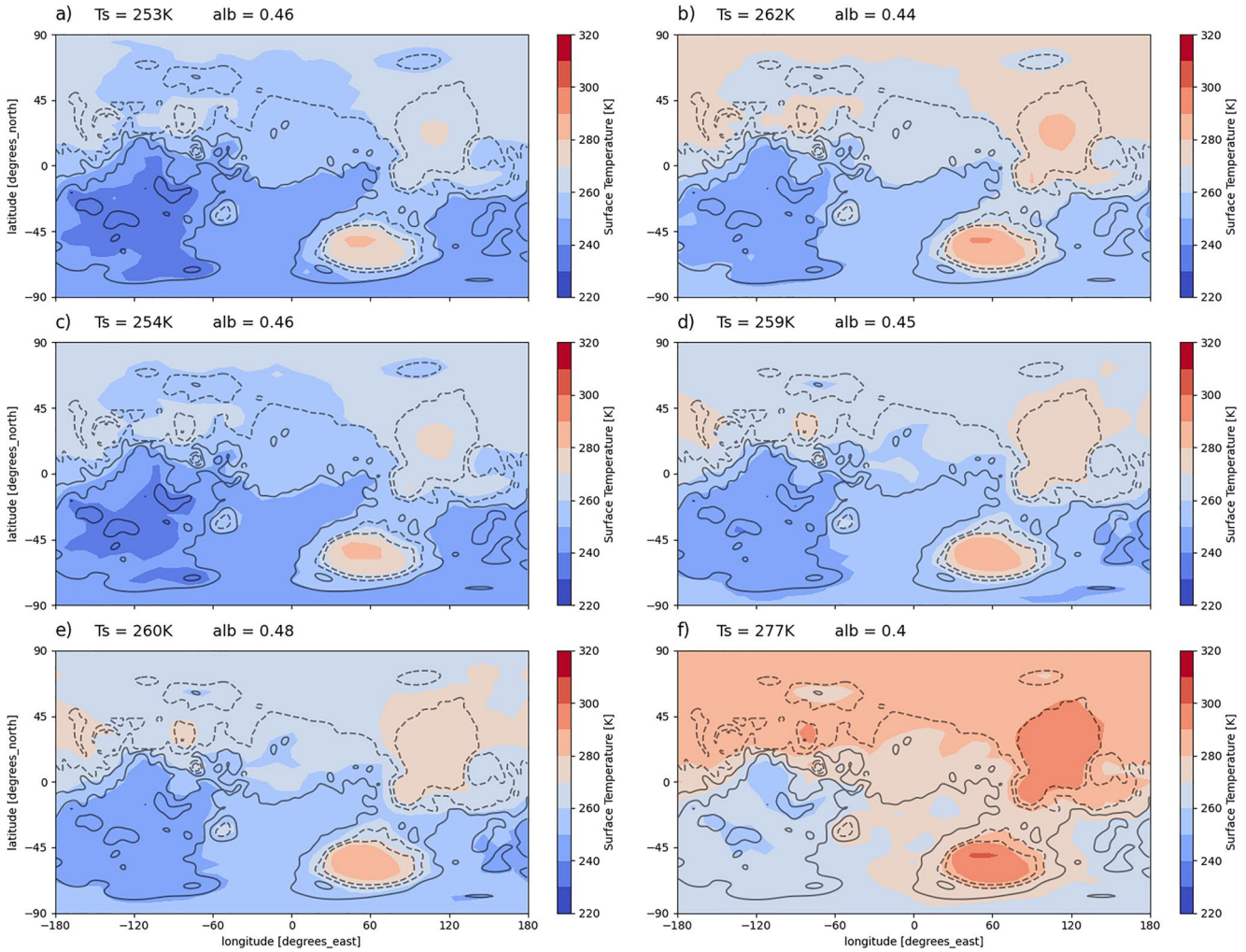

Figure 3. Annual mean surface temperature for an arid scenario with a mean surface pressure of 2 bar *sursat* and *plim* are the two parameters of the supersaturation model, respectively, for the maximum supersaturation ratio allowed and the maximum pressure where supersaturation can occur. p_s stands for surface pressure. (a) Reference simulation, *sursat* = 1; (b) *sursat* = 10, *plim* = p_s; (c) *sursat* = 10, *plim* = 0.5 bar; (d) *sursat* = 10, *plim* 1 bar; (e) *sursat* = 1,000, *plim* = 0.5 bar; (f) *sursat* = 100, *plim* = p_s Global mean surface temperature and Bond albedo are indicated.

having a strong supersaturation in the dusty lower layers of the atmosphere is very unlikely. If the pressure of a given layer is higher than *plim*, the supersaturation ratio is set to be equal to 1 (saturation). In these 1D simulations, the water mixing ratio is not free to evolve and is at least the mixing ratio at saturation.

2.2.2. Supersaturation in the 3D Model

In order to allow supersaturation, the model has been modified where condensation and cloud formation are involved. Cloud formation is mainly described by a large-scale condensation scheme, a moist convective adjustment (Manabe & Wetherald, 1967), and vertical mixing of the boundary layer (Turbet et al., 2017; Wordsworth et al., 2013). In the large-scale condensation scheme, condensation occurs when the water mass mixing ratio is above a relative humidity $RH = 100\%$ or $RH = sursat \times 100\%$ ($sursat \geq 1$) depending on the pressure of the layer and the *plim* parameter, similar to the description of the 1D model.

3. Results

3.1. 1D Model

Figure 1 shows the evolution of the surface temperature of our 1D model with the supersaturation parameter *sursat*. Two sets of simulations are shown. The blue line represented by dots shows the results obtained with

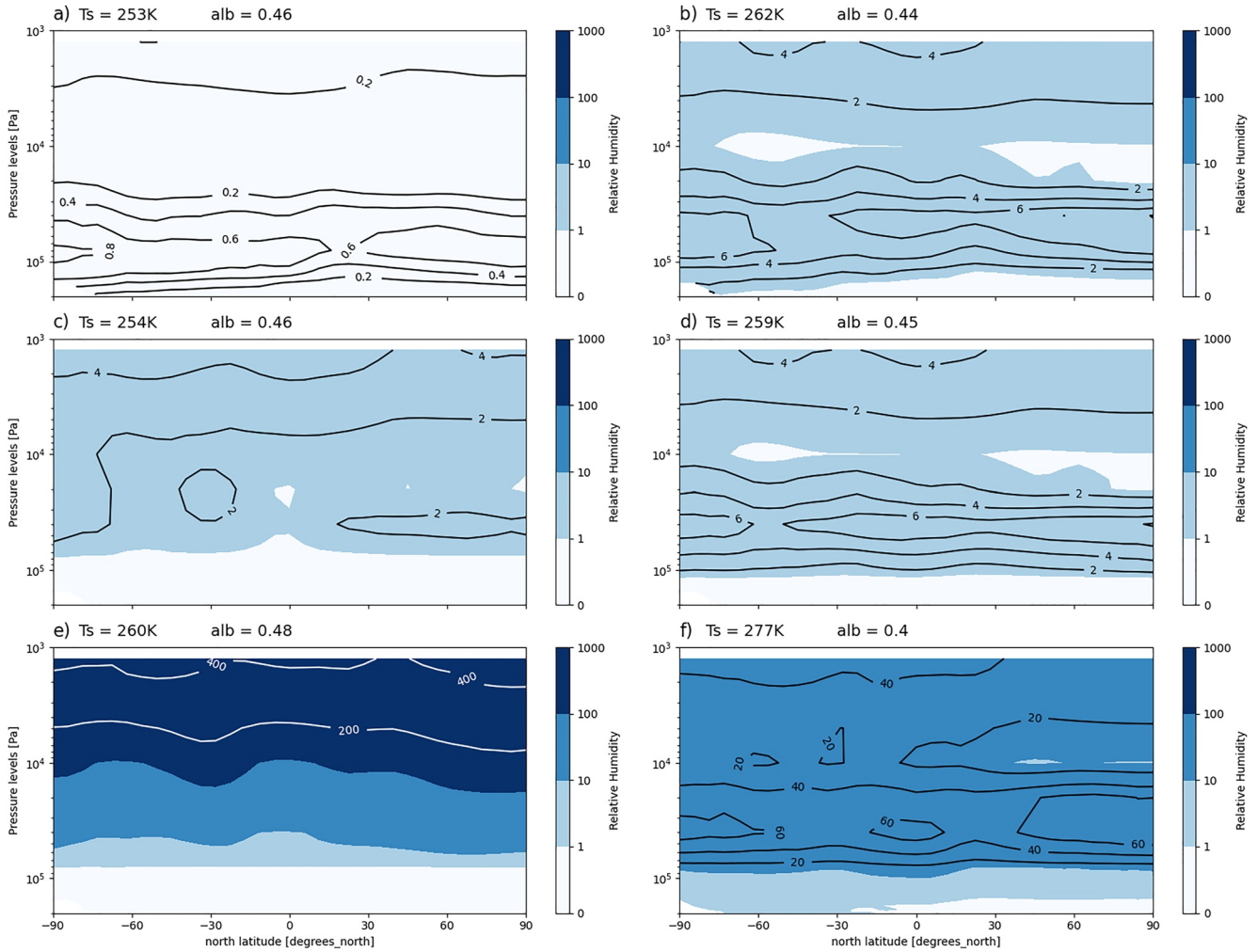

Figure 4. Annual and zonal mean relative humidity (no unit, not in percentage) for an arid scenario with a mean surface pressure of 2 bar *sursat* and *plim* are the two parameters of the supersaturation model, respectively for the maximum supersaturation ratio allowed and the maximum pressure where supersaturation can occur. p_s stands for surface pressure. (a) Reference simulation, *sursat* = 1; (b) *sursat* = 10, *plim* = p_s; (c) *sursat* = 10, *plim* = 0.5 bar; (d) *sursat* = 10, *plim* 1 bar; (e) *sursat* = 1,000, *plim* = 0.5 bar; (f) *sursat* = 100, *plim* = p_s. Global mean surface temperature and Bond albedo are indicated.

radiatively active CO_2 clouds, the crossed orange line being with radiatively inactive clouds. It can be inferred that there is no major feedback of supersaturation on the greenhouse effect of CO_2 clouds with the chosen microphysics parameters, the difference between the two curves being almost constant. Surface temperature reaches the freezing point of water for a supersaturation ratio around 10. Since the surface pressure is 2 bar, it requires lower layers to be supersaturated at levels much higher than what is observed today in cirrus clouds, which can be seen as unrealistic. We can observe supersaturation levels greater than 10 on today's Mars but the pressure is much lower where this occurs (Maltagliati et al., 2011).

Figure 2 illustrates the need for supersaturation to occur in the lower layers in order to have a significant greenhouse effect. The effect of supersaturation is limited to a few Kelvin if it is only above 1 bar (~8 km) and there is no effect if it occurs only above 0.5 bar (~17 km).

We can observe significant warming with *plim* < 0.5 bar only for a high supersaturation ratio. For example, simulations reach a surface temperature of 282 K (275 K) for a *sursat* ratio of 10^5 and a *plim* parameter of 0.2 bar (0.1 bar), respectively. This scenario would imply a high production of H_2O in the upper layers of the atmosphere and not just transport of water from the surface to higher layers.

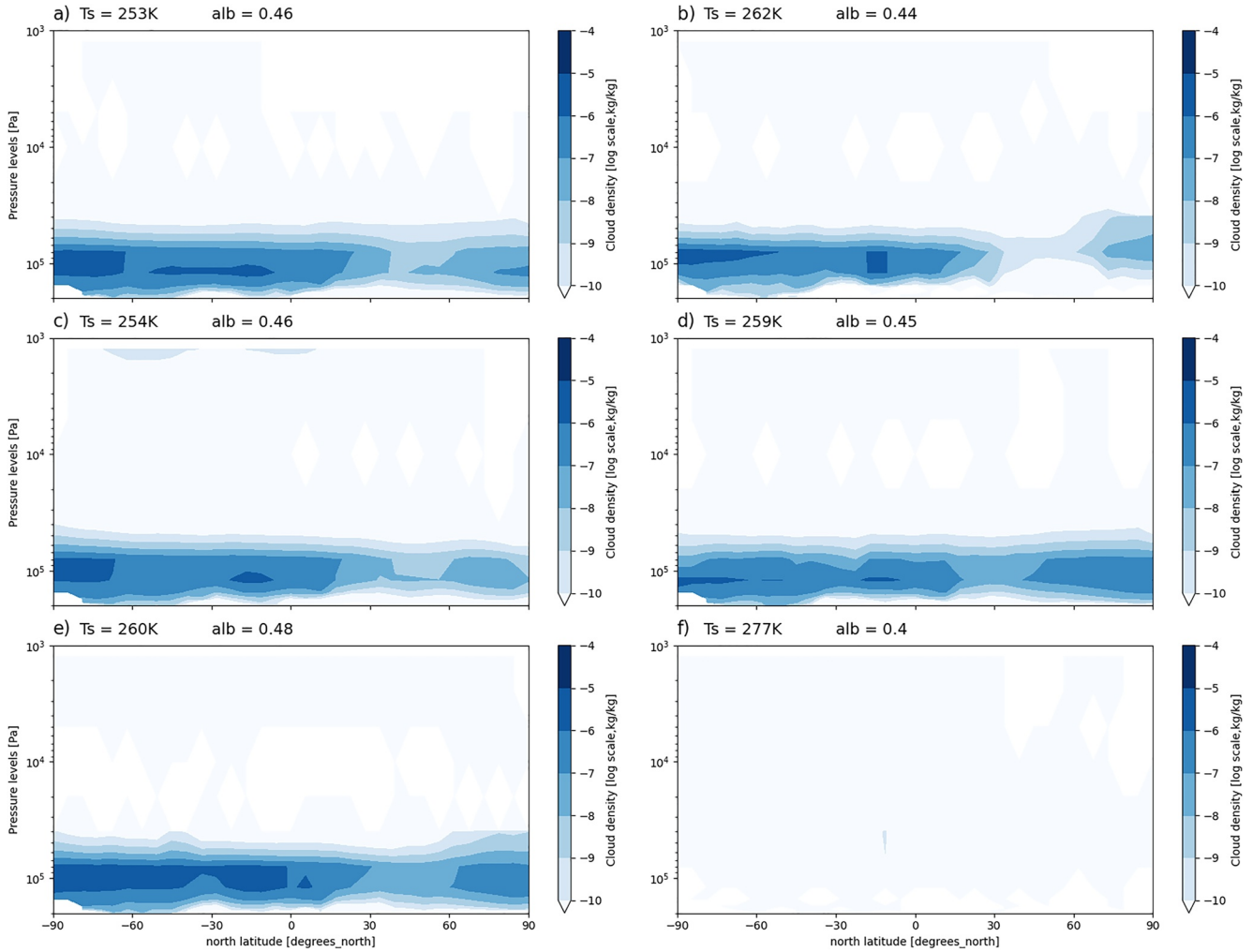

Figure 5. Annual and zonal mean water ice cloud density (kg/kg, log scale) for an arid scenario with a mean surface pressure of 2 bar *sursat* and *plim* are the two parameters of the supersaturation model, respectively for the maximum supersaturation ratio allowed and the maximum pressure where supersaturation can occur. p_s stands for surface pressure. (a) Reference simulation, *sursat* = 1; (b) *sursat* = 10, *plim* = p_s; (c) *sursat* = 10, *plim* = 0.5 bar; (d) *sursat* = 10, *plim* 1 bar; (e) *sursat* = 1,000, *plim* = 0.5 bar; (f) *sursat* = 100, *plim* = p_s. Global mean surface temperature and Bond albedo are indicated.

3.2. Effect of Supersaturation in 3D Models

The 1D results suggest that water supersaturation could warm early Mars, assuming that it occurred everywhere and especially in the lower atmosphere. To further investigate if this is possible, and to explore the feedback between clouds and supersaturation, a 3D model is needed.

3.2.1. Arid Simulation

The first set of simulations is performed with a mean surface pressure of 2 bar and relatively dry initial conditions as described in Section 2.1. Water ice is mainly located in the elevated regions near the current location of Tharsis (Bouley et al., 2016, Figure 2) and the global water content is 33 mm GEL, mainly of ice on the surface (with only 10 pr-μm of water ice clouds, 390 pr-μm of water vapor). A reference simulation is performed without supersaturation. The average mean temperature is 253 K, consistent with Wordsworth et al. (2013). Figure 3 shows the mean annual surface temperature for different simulations performed from this dry initial state. In Figures 4 and 5, the relative humidity *RH* and cloud density are shown, respectively, for the same simulations. Global mean temperature and planetary albedo are indicated for these simulations.

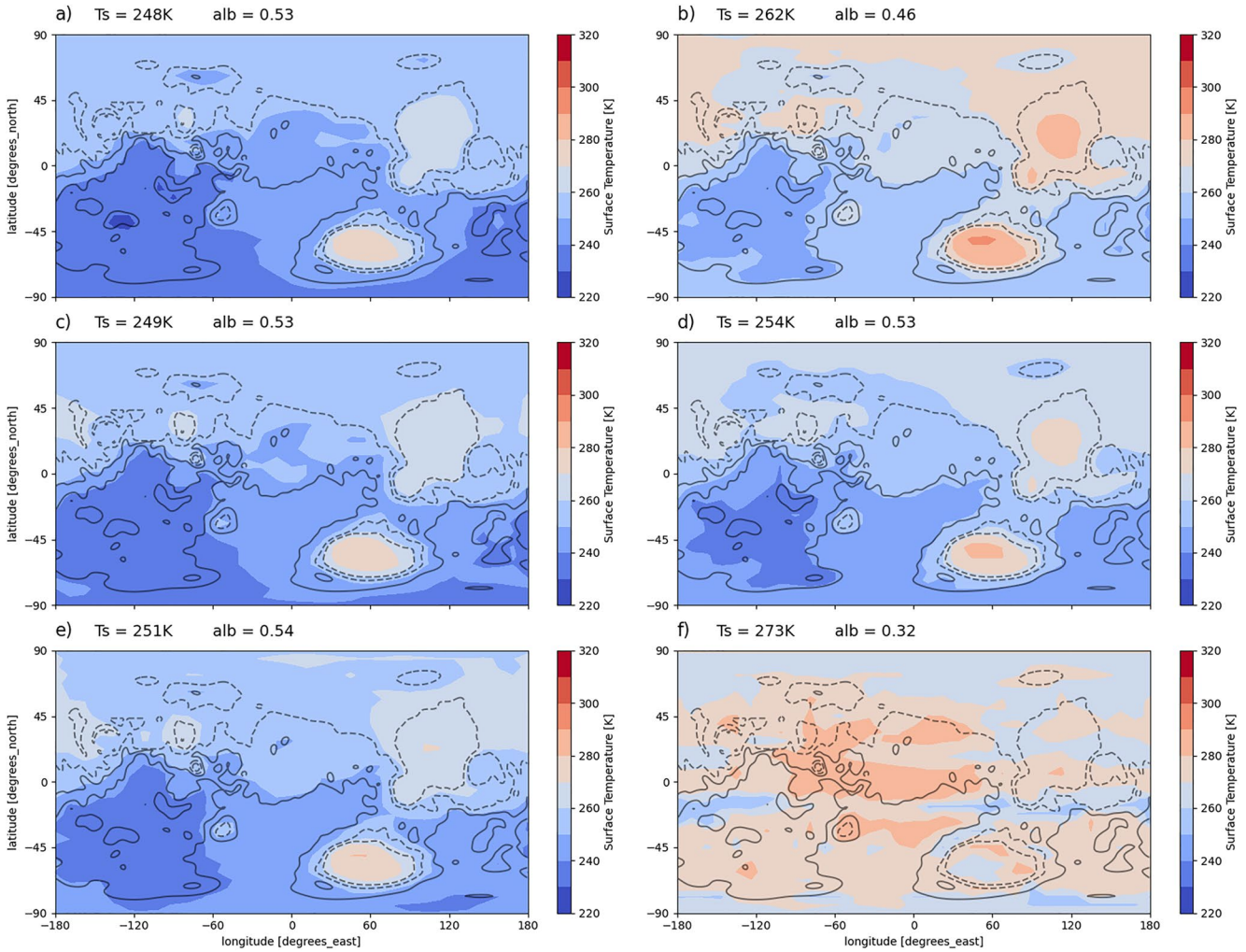

Figure 6. Annual mean surface temperature for an idealized wet scenario with a mean surface pressure of 2 bar. *sursat* and *plim* are the two parameters of the supersaturation model, respectively for the maximum supersaturation ratio allowed and the maximum pressure where supersaturation can occur. p_s stands for surface pressure. (a) Reference simulation, *sursat* = 1; (b) *sursat* = 10, *plim* = p_s; (c) *sursat* = 10, *plim* = 0.5 bar; (d) *sursat* = 10, *plim* 1 bar; (e) *sursat* = 1,000, *plim* = 0.5 bar; (f) *sursat* = 100, *plim* = p_s. Global mean surface temperature and Bond albedo are indicated.

As expected for such surface pressure (Forget et al., 2013, Figure 7), local surface temperatures are influenced by adiabatic warming and cooling mechanisms and we can see that the northern plains are globally warmer (around 20 K) than the southern hemisphere, except for the Hellas basin, for all simulations. As expected from the 1D study (Figure 2), supersaturation is only efficient when it occurs in the lower layers of the atmosphere. Here, for a *sursat* parameter of 10 (as in 3b–3d), there is almost no warming when supersaturation is assumed only above the 0.5 bar level. Figure 3e confirms that, even with a high supersaturation ratio, there is no significant warming if the *plim* parameter is less than 0.5 bar. A simulation with an even higher *sursat* ratio (not shown) does not present significantly higher temperatures since water vapor struggles to reach the higher layers of the atmosphere.

Annual and zonal mean relative humidity profiles are shown in Figure 4. The reference simulation (Figure 3a) depicts a maximum zone of relative humidity between 0.5 and 1 bar. This optimum zone corresponds to a hygropause (see Figure 5) and the higher layers above 0.1 bar are relatively dry. A similar pattern is observed for simulations where supersaturation is uniformly allowed down to the surface (Figures 3b and 3f). If supersaturation is allowed only from 1 bar (Figure 3d), the wet area is thinner and it even vanishes when supersaturation is allowed only from 0.5 bar (Figures 3c and 3e). As a consequence, our simulations can not fully supersaturate the layers above 0.5 bar and are unable to create a significant warming even with a high supersaturation ratio.

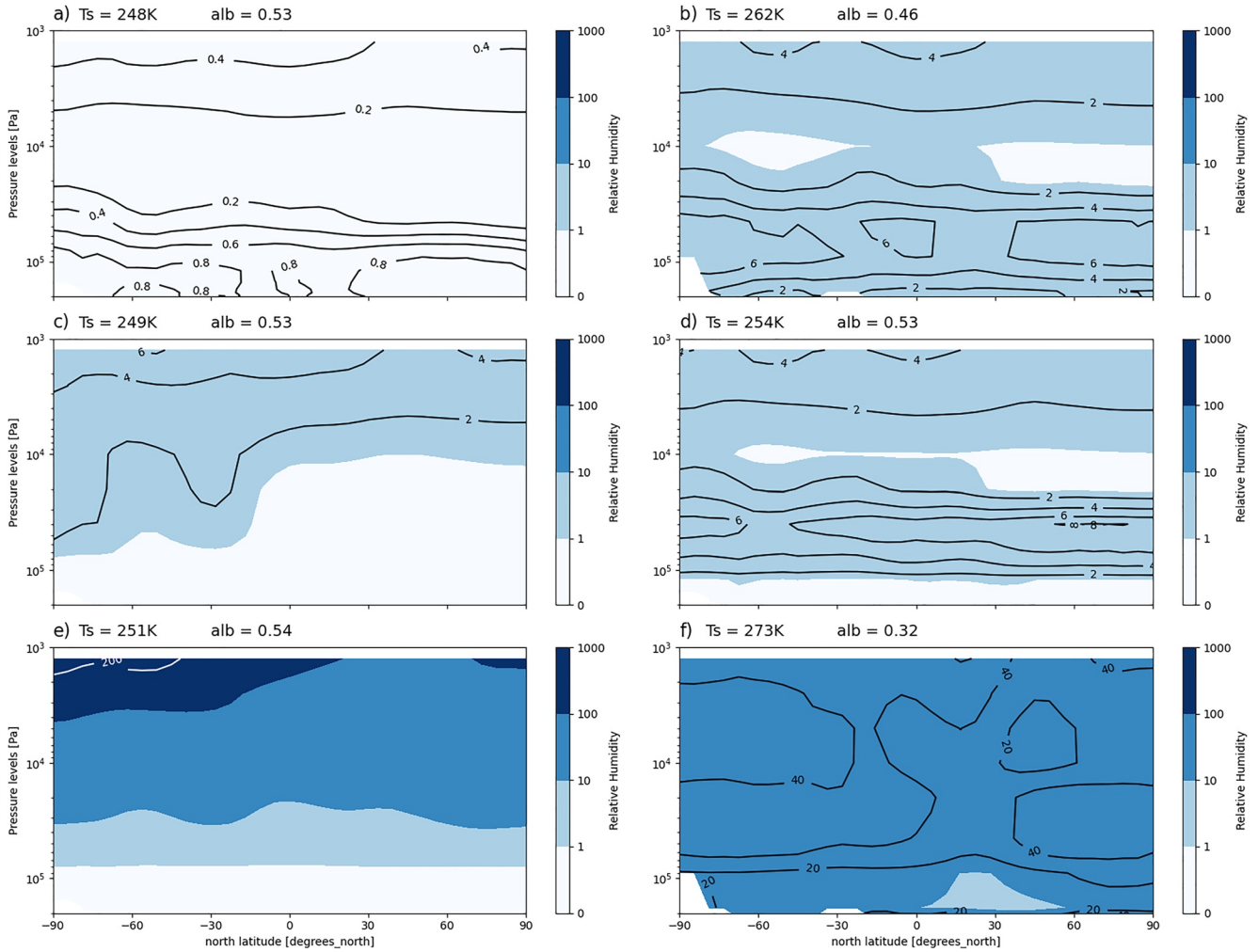

Figure 7. Annual and zonal mean relative humidity (no unit, not in percentage) for an idealized wet scenario with a mean surface pressure of 2 bar. *sursat* and *plim* are the two parameters of the supersaturation model, respectively for the maximum supersaturation ratio allowed and the maximum pressure where supersaturation can occur. p_s stands for surface pressure. (a) Reference simulation, *sursat* = 1; (b) *sursat* = 10, *plim* = p_s; (c) *sursat* = 10, *plim* = 0.5 bar; (d) *sursat* = 10, *plim* 1 bar; (e) *sursat* = 1,000, *plim* = 0.5 bar; (f) *sursat* = 100, *plim* = p_s. Global mean surface temperature and Bond albedo are indicated.

Zonally and annually averaged cloud density is shown in Figure 5. In the reference simulation (Figure 5a), clouds are mainly located around the pressure level of 1 bar and vertically limited by a hygropause at approximately 0.5 bar. The pattern is identical for simulations with *sursat* ≤ 1 bar (Figures 5c–5e) and we observe a slight shift toward higher altitudes when *plim* = p_s (Figure 5b). For the extreme case simulation with *sursat* = 100 and supersaturation allowed from the surface (Figure 5f), water clouds are totally removed from the atmosphere. A simulation similar to the reference simulation but performed without the radiative effect of clouds (not shown) shows that clouds have a limited impact on the global surface temperature. Thus, in the case of arid simulations, the warming observed with high *sursat* values is fully related to the quantity of water vapor in the atmosphere, which absorbs the emitted IR flux.

3.2.2. Idealized Wet Simulation

This scenario is designed to maximize the amount of water vapor in the atmosphere, assuming that there is no significant photochemical source in the atmosphere. Although this is not physically realistic, because we set an unusually low albedo for the ice (0.2, typical of bare soil), this scenario allows us to explore if the atmospheric circulation limits the amount of water vapor when surface sources are abundant. Similar to the arid scenario, Figures 6–8, respectively, describe annual mean surface temperature, zonal and annual average relative humidity and cloud density. Even with water content significantly higher in this idealized wet scenario (see Table 1), the

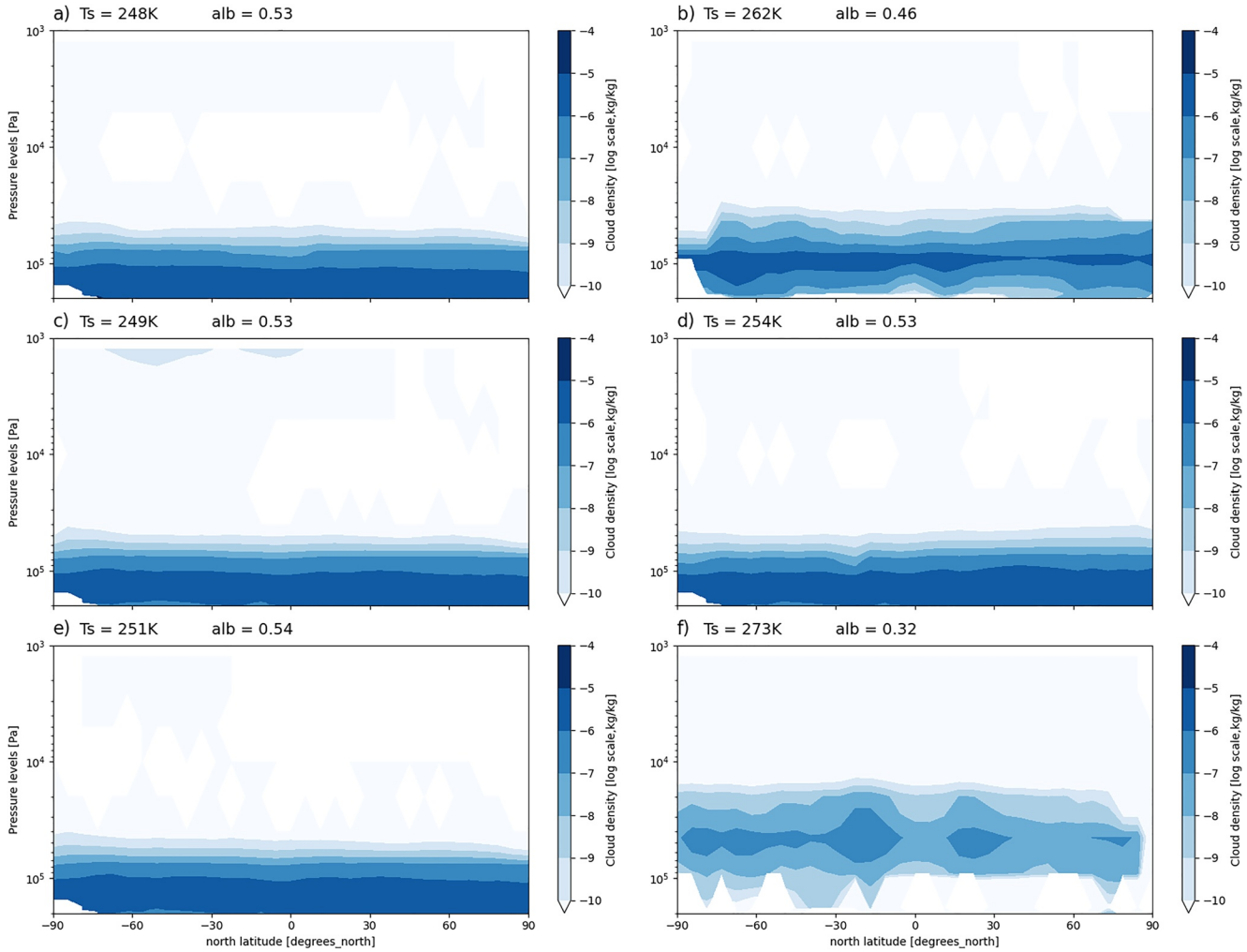

Figure 8. Annual and zonal mean water ice cloud density (kg/kg, log scale) for an idealized wet scenario with a mean surface pressure of 2 bar. *sursat* and *plim* are the two parameters of the supersaturation model, respectively for the maximum supersaturation ratio allowed and the maximum pressure where supersaturation can occur. p_s stands for surface pressure. (a) Reference simulation, *sursat* = 1; (b) *sursat* = 10, *plim* = p_s; (c) *sursat* = 10, *plim* = 0.5 bar; (d) *sursat* = 10, *plim* 1 bar; (e) *sursat* = 1,000, *plim* = 0.5 bar; (f) *sursat* = 100, *plim* = p_s. Global mean surface temperature and Bond albedo are indicated.

simulations are not able to reach a global mean surface temperature above the freezing point of water, except for the *sursat* = 100 simulation, which is described further. Surface temperatures are even slightly colder than in the arid scenario.

Surface temperatures are lower mainly because of the high albedo of clouds that cover a large part of the planet. This negative feedback is not compensated by a strong greenhouse effect. As shown in Figure 8, the high amount of water injected into the atmosphere from the initial ice sheet creates thick and low clouds (Figures 8a, 8c–8e) with a net cooling effect. Supersaturation is able to raise the formation altitude of the clouds and reduce the total planetary albedo (Figures 8b and 8f), but only when supersaturation is allowed from the ground to the top of the atmosphere.

Similar to the arid scenario, we observe that water vapor is not fully supersaturated in the highest levels of the atmosphere, especially for simulations with low *sursat* or *plim* parameters (Figure 7). The simulation with a high *sursat* ratio (Figure 7e) reaches slightly lower relative humidity in the upper layers compared to the arid simulation and still is not able to provide a significant warming, despite our ambition to model a more humid atmosphere in this scenario. As a consequence, we are not able to create a highly supersaturated layer in the upper atmosphere as is done in Ito et al. (2020) with H_2O_2.

Table 1
Yearly Global Water Content (kg/m²)

Simulation	Surface ice	Clouds particles	Vapor
DRY Ref	32.6	0.010	0.4
DRY S10	28.8	0.007	4.0
IC Ref	9,938	0.10	1.6
IC S10	9,986	0.06	16.3

The extreme case presented in Figure 7f is surprising in the fact that the surface temperature pattern is not similar to the other simulations. In fact, due to the high quantities of water in the layers where the pressure is above 2 bar, we observe a decrease in the incident solar flux at the surface due to the absorption by the water vapor in the solar spectrum range. This creates a pattern where low-altitude regions such as the Hellas basin or Elysium Planitia have lower surface temperatures than areas located at higher altitudes. The effect of a high *sursat* ratio is interesting regarding clouds because it raises the altitude of clouds, which are also less dense. The global result is a lower cooling effect of clouds, since high cirrus clouds are expected to create a stronger greenhouse effect (Ramirez & Kasting, 2017). This simulation shows a global mean surface temperature above the freezing point of water and, more interestingly, in the southern areas, where valley networks are currently observed. However, the supersaturation levels and the quantity of water in the atmosphere are totally unrealistic.

4. Conclusions

Using 1D and 3D global climate models, We investigated the potential impact of a water supersaturation on warming a CO_2-dominated atmosphere on early Mars. Our 1D results showed that supersaturation could warm the planet considering a high supersaturation ratio in every layer of the atmosphere, especially the lower layers. This conclusion is tempered by 3D results, where we reached a relevant warming only with a highly unrealistic supersaturation ratio in the lower layers of a dense atmosphere.

Additionally, we demonstrated that supersaturation can create higher altitude clouds both in our arid and idealized wet simulation with water sources on the surface. However, this increase in the height of water clouds is seen only with supersaturation occurring from the ground, and is not enough to create a sustainable warming of the surface in most of our simulations. An extreme case with an unrealistic supersaturation ratio of 100 creates a significant warming associated with a high amount of water vapor in the atmosphere and a higher cloud layer.

Data Availability Statement

Data files for figures used in this analysis are available in a public repository, see Delavois et al. (2022).

Acknowledgments
This project received funding from the European Research Council (ERC) under the European Union's Horizon 2020 research and innovation programme (grant agreement No 835275). The authors acknowledge the exceptional computing support from Grand Equipement National de Calcul Intensif (GENCI) and Centre Informatique National de l'Enseignement Supérieur (CINES). All the simulations presented here were carried out on the Occigen cluster hosted at CINES.

References

Baumgartner, M., Rolf, C., Grooß, J.-U., Schneider, J., Schorr, T., Möhler, O., et al. (2022). New investigations on homogeneous ice nucleation: The effects of water activity and water saturation formulations. *Atmospheric Chemistry and Physics*, *22*(1), 65–91. https://doi.org/10.5194/acp-22-65-2022

Bouley, S., Baratoux, D., Matsuyama, I., Forget, F., Séjourné, A., Turbet, M., & Costard, F. (2016). Late Tharsis formation and implications for early Mars. *Nature*, *531*(7594), 344–347. https://doi.org/10.1038/nature17171

Delavois, A., Forget, F., Turbet, M., Millour, E., Vandemeulebrouck, R., Lange, L., & Bierjon, A. (2022). Water supersaturation for early Mars [Dataset]. DVN. https://doi.org/10.7910/DVN/O94VWV

Fedorova, A., Bertaux, J.-L., Betsis, D., Montmessin, F., Korablev, O., Maltagliati, L., & Clarke, J. (2018). Water vapor in the middle atmosphere of Mars during the 2007 global dust storm. *Icarus*, *300*, 440–457. https://doi.org/10.1016/j.icarus.2017.09.025

Fedorova, A., Montmessin, F., Korablev, O., Luginin, M., Trokhimovskiy, A., Belyaev, D. A., et al. (2020). Stormy water on Mars: The distribution and saturation of atmospheric water during the dusty season. *Science*, *367*(6475), 297–300. https://doi.org/10.1126/science.aay9522

Forget, F., Wordsworth, R., Millour, E., Madeleine, J. B., Kerber, L., Leconte, J., et al. (2013). 3D modelling of the early Martian climate under a denser CO_2 atmosphere: Temperatures and CO_2 ice clouds. *Icarus*, *222*(1), 81–99. https://doi.org/10.1016/j.icarus.2012.10.019

Genthon, C., Piard, L., Vignon, E., Madeleine, J.-B., Casado, M., & Gallée, H. (2017). Atmospheric moisture supersaturation in the near-surface atmosphere at Dome C, Antarctic Plateau. *Atmospheric Chemistry and Physics*, *17*(1), 691–704. https://doi.org/10.5194/acp-17-691-2017

Gough, D. O. (1981). Solar interior structure and luminosity variations. *Solar Physics*, *74*(1), 21–34. https://doi.org/10.1007/BF00151270

Heymsfield, A. J., Krämer, M., Luebke, A., Brown, P., Cziczo, D. J., Franklin, C., et al. (2017). Cirrus clouds. *Meteorological Monographs*, *58*(1), 2.1–2.26. https://doi.org/10.1175/AMSMONOGRAPHS-D-16-0010.1

Ito, Y., Hashimoto, G. L., Takahashi, Y. O., Ishiwatari, M., & Kuramoto, K. (2020). H_2O_2-induced greenhouse warming on oxidized early Mars. *The Astrophysical Journal*, *893*(2), 168. https://doi.org/10.3847/1538-4357/ab7db4

Kamada, A., Kuroda, T., Kasaba, Y., Terada, N., & Nakagawa, H. (2021). Global climate and river transport simulations of early Mars around the Noachian and Hesperian boundary. *Icarus*, *368*, 114618. https://doi.org/10.1016/j.icarus.2021.114618

Kite, E. S., Steele, L. J., Mischna, M. A., & Richardson, M. I. (2021). Warm early Mars surface enabled by high-altitude water ice clouds. *Proceedings of the National Academy of Sciences of the United States of America*, *118*(18), 2101959118. https://doi.org/10.1073/pnas.2101959118

Krämer, M., Rolf, C., Spelten, N., Afchine, A., Fahey, D., Jensen, E., et al. (2020). A microphysics guide to cirrus—Part 2: Climatologies of clouds and humidity from observations. *Atmospheric Chemistry and Physics*, *20*(21), 12569–12608. https://doi.org/10.5194/acp-20-12569-2020

Krämer, M., Schiller, C., Afchine, A., Bauer, R., Gensch, I., Mangold, A., et al. (2009). Ice supersaturations and cirrus cloud crystal numbers. *Atmospheric Chemistry and Physics*, *9*(11), 3505–3522. https://doi.org/10.5194/acp-9-3505-2009

Lamquin, N., Stubenrauch, C. J., Gierens, K., Burkhardt, U., & Smit, H. (2012). A global climatology of upper-tropospheric ice supersaturation occurrence inferred from the Atmospheric Infrared Sounder calibrated by MOZAIC. *Atmospheric Chemistry and Physics*, *12*(1), 381–405. https://doi.org/10.5194/acp-12-381-2012

Lanza, N. L., Wiens, R. C., Arvidson, R. E., Clark, B. C., Fischer, W. W., Gellert, R., et al. (2016). Oxidation of manganese in an ancient aquifer, Kimberley formation, Gale crater, Mars. *Geophysical Research Letters*, *43*(14), 7398–7407. https://doi.org/10.1002/2016GL069109

Maltagliati, L., Montmessin, F., Fedorova, A., Korablev, O., Forget, F., & Bertaux, J. L. (2011). Evidence of water vapor in excess of saturation in the atmosphere of Mars. *Science*, *333*(6051), 1868–1871. https://doi.org/10.1126/science.1207957

Manabe, S., & Wetherald, R. T. (1967). Thermal equilibrium of the atmosphere with a given distribution of relative humidity. *Journal of the Atmospheric Sciences*, *24*(3), 241–259. https://doi.org/10.1175/1520-0469(1967)024⟨0241:TEOTAW⟩2.0.CO;2

Murray, B. J., & Jensen, E. J. (2010). Homogeneous nucleation of amorphous solid water particles in the upper mesosphere. *Journal of Atmospheric and Solar-Terrestrial Physics*, *72*(1), 51–61. https://doi.org/10.1016/j.jastp.2009.10.007

Poncin, L., Kleinböhl, A., Kass, D. M., Clancy, R. T., Aoki, S., & Vandaele, A. C. (2022). Water vapor saturation and ice cloud occurrence in the atmosphere of Mars. *Planetary and Space Science*, *212*, 105390. https://doi.org/10.1016/j.pss.2021.105390

Ramirez, R. M. (2017). A warmer and wetter solution for early Mars and the challenges with transient warming. *Icarus*, *297*, 71–82. https://doi.org/10.1016/j.icarus.2017.06.025

Ramirez, R. M., & Kasting, J. F. (2017). Could cirrus clouds have warmed early Mars? *Icarus*, *281*, 248–261. https://doi.org/10.1016/j.icarus.2016.08.016

Ramirez, R. M., Kopparapu, R., Zugger, M. E., Robinson, T. D., Freedman, R., & Kasting, J. F. (2014). Warming early Mars with CO_2 and H_2. *Nature Geoscience*, *7*(1), 59–63. https://doi.org/10.1038/ngeo2000

Sagan, C., & Mullen, G. (1972). Earth and Mars: Evolution of atmospheres and surface temperatures. *Science*, *177*(4043), 52–56. https://doi.org/10.1126/science.177.4043.52

Segura, T. L., McKay, C. P., & Toon, O. B. (2012). An impact-induced, stable, runaway climate on Mars. *Icarus*, *220*(1), 144–148. https://doi.org/10.1016/j.icarus.2012.04.013

Segura, T. L., Toon, O. B., & Colaprete, A. (2008). Modeling the environmental effects of moderate-sized impacts on Mars. *Journal of Geophysical Research*, *113*(E11), E11007. https://doi.org/10.1029/2008JE003147

Segura, T. L., Toon, O. B., Colaprete, A., & Zahnle, K. (2002). Environmental effects of large impacts on Mars. *Science*, *298*(5600), 1977–1980. https://doi.org/10.1126/science.1073586

Turbet, M., & Forget, F. (2019). The paradoxes of the Late Hesperian Mars ocean. *Scientific Reports*, *9*(1), 5717. https://doi.org/10.1038/s41598-019-42030-2

Turbet, M., & Forget, F. (2022). 3-D Global modelling of the early Martian climate under a dense CO_2+H_2 atmosphere and for a wide range of surface water inventories (Tech. Rep.). Retrieved from https://ui.adsabs.harvard.edu/abs/2021arXiv210310301T

Turbet, M., Forget, F., Head, J. W., & Wordsworth, R. (2017). 3D modelling of the climatic impact of outflow channel formation events on early Mars. *Icarus*, *288*, 10–36. https://doi.org/10.1016/j.icarus.2017.01.024

Urata, R. A., & Toon, O. B. (2013). Simulations of the Martian hydrologic cycle with a general circulation model: Implications for the ancient Martian climate. *Icarus*, *226*(1), 229–250. https://doi.org/10.1016/j.icarus.2013.05.014

Vali, G., DeMott, P. J., Möhler, O., & Whale, T. F. (2015). Technical note: A proposal for ice nucleation terminology. *Atmospheric Chemistry and Physics*, *15*(18), 10263–10270. https://doi.org/10.5194/acp-15-10263-2015

Wordsworth, R., Forget, F., Millour, E., Head, J. W., Madeleine, J. B., & Charnay, B. (2013). Global modelling of the early Martian climate under a denser CO_2 atmosphere: Water cycle and ice evolution. *Icarus*, *222*, 1–19. https://doi.org/10.1016/j.icarus.2012.09.036

Wordsworth, R. D. (2016). The climate of early Mars. *Annual Review of Earth and Planetary Sciences*, *44*(1), 381–408. https://doi.org/10.1146/annurev-earth-060115-012355